ACS OMEGA

Open Access

http://pubs.acs.org/journal/acsodf

Article

Highly Sensitive Room Temperature H_2S Gas Sensor Based on the Nanocomposite of MoS_2−$ZnCo_2O_4$

Shama Sadaf, Hongpeng Zhang,* Daru Chen,* and Ali Akhtar*

Cite This: *ACS Omega* 2023, 8, 47023−47033

Read Online

ACCESS | Metrics & More | Article Recommendations

ABSTRACT: The stacking 2D materials, such as molybdenum disulfide (MoS_2), are among the most promising candidates for detecting H_2S gas. Herein, we designed a series of novel nanocomposites consisting of MoS_2 and $ZnCo_2O_4$. These materials were synthesized via a simple hydrothermal method. The microstructure and morphology of nanocomposites were studied by different characteristics such as X-ray diffraction, scanning electron microscopy, energy-dispersive X-ray spectroscopy, transmission electron microscopy, high-resolution transmission electron microscopy, Brunauer−Emmett−Teller (BET), and X-ray photoelectron spectroscopy. These nanocomposites were used as gas sensors, and the highest response (6.6) toward 10 ppm of H_2S was detected by the gas sensor of MZCO-6 (having MoS_2 contents 0.060 g) among all other tested sensors. The response value (R_a/R_g) was almost three times that of pure $ZnCo_2O_4$ (R_a/R_g = 2). In addition, the sensor of MZCO-6 exposed good selectivity, short response/recovery time (12/28 s), long-term stability (28 days), and a low detection limit (0.5 ppm) toward H_2S gas at RT. The excellent performance of MZCO-6 may be attributed to some features of MoS_2, such as stack structure, higher BET and surface area and active sites, a synergistic effect, etc. This simple fabrication sensor provides a novel idea for detecting H_2S gas at RT.

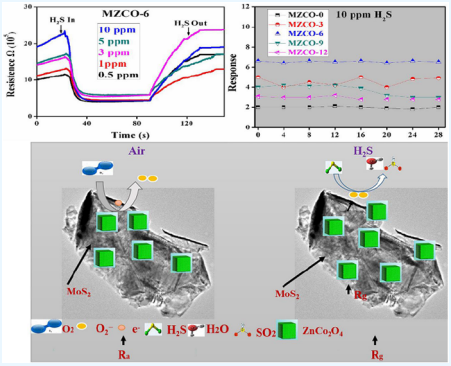

1. INTRODUCTION

Detecting hazardous and flammable gases, such as hydrogen sulfide (H_2S) with rotten egg smell, is important for protecting human health. It is also called industrial exhaust gas, which is usually produced in industries, cooking ovens, kitchen waste, wastewater treatment centers, sewers, and oil and gas fields.[1] The excessive inhalation of H_2S, around 250 ppm, may cause the death of human beings;[2] besides, very low concentration of H_2S than above-mentioned ones can cause various chronic diseases such as poor memory, throat injury, dizziness, and cough and affect human nervous system as well.[3] In this regard, H_2S gas sensors with a high response and low limit of detection (LOD) are highly required.

Semiconductor metal oxides (SMOs) are highly recommended and studied as gas sensors because of their advantages of low cost, simple fabrication, small size, and ability to synthesize various nanocomposites.[4] Up to now, different SMOs, such as NiO, CuO, $NiCo_2O_4$, and $ZnCo_2O_4$, have received wide attention in the field of gas sensors.[5−8] Among these SMOs, $ZnCo_2O_4$, an important functional material, can design novel composites with different metal oxides due to its special spinel structure. $ZnCo_2O_4$ having a band gap of 2.6 eV was found to be a promising candidate for detecting various gases such as H_2S,[9] acetone,[10] triethylamine,[11] ethylene glycol,[12] and formaldehyde.[13] However, the reported gas sensors of $ZnCo_2O_4$ still need improvement due to some demerits such as high temperature, low response, poor selectivity, etc. Designing novel nanocomposites of $ZnCo_2O_4$ with stacks of 2D materials is crucial to achieving these objectives.

Molybdenum disulfide (MoS_2), a n-type semiconductor having a band gap of 1.29 eV, is one of the most well-known 2D material of transition-metal dichalcogenide family; especially, the stacking structure of 2D materials has received great attention because of strong adsorption, high reactivity, larger surface area-to-volume ratio, and good electrical conductivity.[14] Except for the gas sensors, it has been used in many fields, such as photocatalysis,[15] supercapacitor,[16] and lithium-ion batteries.[17] It can easily be composited with various SMOs to design novel electronic devices. These features make MoS_2 a very promising candidate for detecting hazardous gases at low concentrations. In particular, Bai and co-workers proposed a sensor based on the heterostructure of MoS_2/SnO_2, which exposed the gas-sensing properties toward NO_2 at room temperature. The optimized sensor showed a high response, short response/recovery (res./rec.) time, good

Received: September 9, 2023
Revised: October 24, 2023
Accepted: November 15, 2023
Published: November 27, 2023

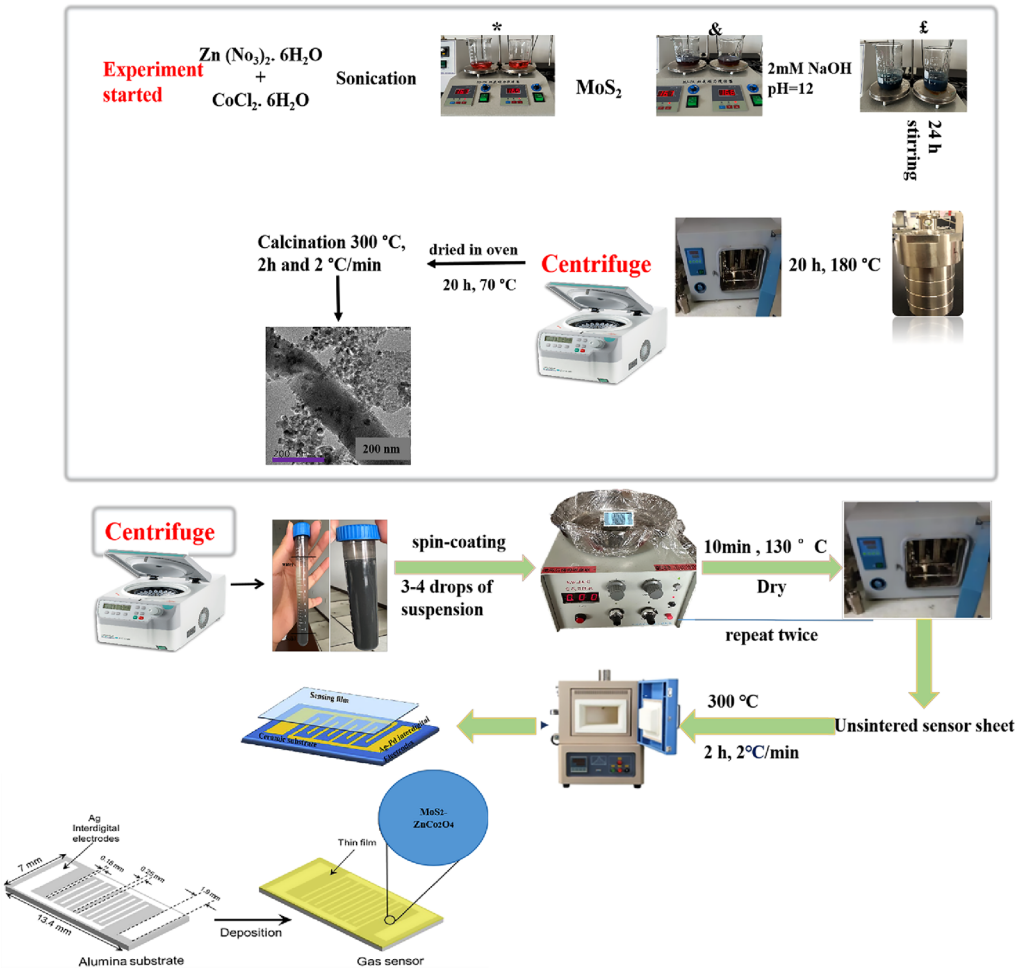

Figure 1. Synthesis diagram and fabrication of the MoS_2−$ZnCo_2O_4$ nanocomposite.

stability, and selectivity. In addition, many sensors such as MoS_2/SnO_2 (CO sensor),[18] CuO/MoS_2 (NO_2 sensor),[19] MoS_2/ZnO (NO_2 sensor),[20] Au/MoS_2 (NO_2 sensor),[21] MoS_2/ZnO-Zn_2SnO_4 (H_2S sensor),[22] and PtO_2/MoS_2 (NH_3 sensor)[23] have been exploited to investigate sub-ppm level gases.

Herein, a series of novel nanocomposites based on $ZnCo_2O_4$ cubes and stacks like MoS_2 were designed for detecting toxic gases. Numerous characterizations such as X-ray diffraction (XRD), scanning electron microscopy (SEM), energy-dispersive X-ray spectroscopy (EDS), transmission electron microscopy (TEM), high-resolution transmission electron microscopy (HETEM), Brunauer−Emmett−Teller (BET), and X-ray photoelectron spectroscopy (XPS) were performed for these nanocomposites. The gas-sensing properties of the proposed sensor of MZCO-6 suggested the high response, good selectivity, short res./rec. time, and reliable long-term stability toward 10 ppm of H_2S among all other tested sensors (MZCO-0, MZCO-3, MZCO-9, and MZCO-12 having MoS_2 contents such as 0.00, 0.030, 0.091, and 0.012 g, respectively, in the nanocomposites). In addition, the gas-sensing properties of MoS_2 were also studied for comparison.

2. EXPERIMENTAL SECTION

2.1. Materials. All of the chemicals used in the synthesis method were bought from Sinopharm Chemical Reagent Co., Ltd. (Shanghai, China). Materials such as MoS_2, cobalt chloride hexahydrate ($CoCl_2{\cdot}6H_2O$), zinc nitrate hexahydrate ($Zn(NO_3)_2{\cdot}\ 6H_2O$), and sodium hydroxide (NaOH) were utilized in the synthesis method without further purification.

2.2. Synthesis of Cube-Shaped $ZnCo_2O_4$ and Nanocomposites of MoS_2−$ZnCo_2O_4$. Cube-shaped $ZnCo_2O_4$ and nanocomposites with different contents of MoS_2 were subsequently synthesized via a simple hydrothermal method, and its detail is expressed in Figure 1. At the start, $CoCl_2{\cdot}6H_2O$ (8 mmol) and $Zn(NO_3)_2{\cdot}\ 6H_2O$ (4 mmol) were mixed with 50 mL deionized water (DI) into five different beakers (diagram, *); after half an hour of stirring, various contents of MoS_2 such as 0.00, 0.030, 0.060, 0.091, and 0.012 g were dispersed into all five suspensions. These samples were named as MZCO-0, MZCO-3, MZCO-6, MZCO-9, and MZCO-12, respectively (diagram, &). After that, 2 mM NaOH was added to adjust pH = 12 (diagram, £). The samples were stirred for 24 h, then on the next day, the mixtures were settled in 50 mL stainless steel autoclaves, and the oven was set at the operating temperature of 180 °C for 20 h. The obtained products were washed with DI and ethanol three times using centrifugation. After drying (20 h, 70 °C), the products were calcined at the operating temperature of 300 °C for 2 h and 2 °C/min. The dried samples, after calcination, were ground in a mortar for different characteristics such as XRD, SEM, TEM, etc. All these tests were performed by providing various amounts of samples, such as 20−30, 10, 10, 10, 200, and 5−20 mg of powder for XRD, SEM, TEM, EDS, BET, and XPS, respectively.

https://doi.org/10.1021/acsomega.3c06876
ACS Omega 2023, 8, 47023−47033

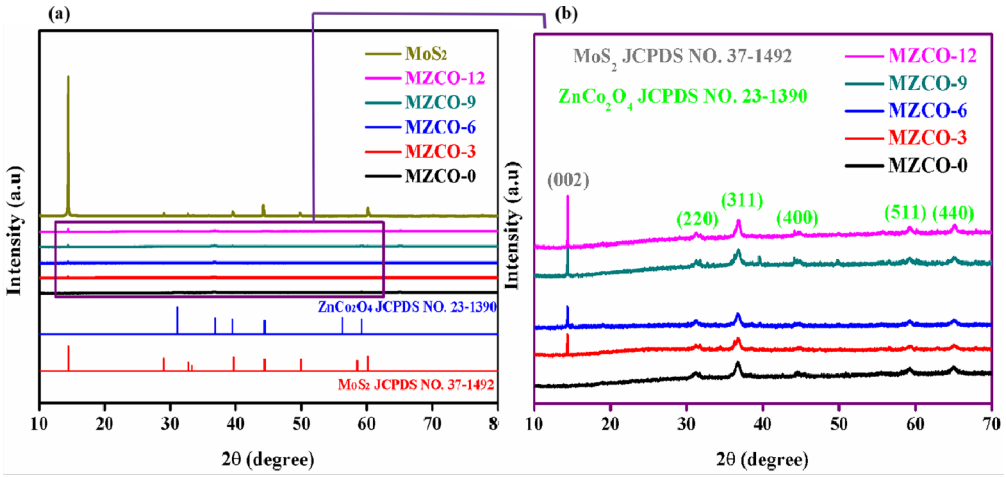

Figure 2. (a,b) XRD patterns of MoS_2−$ZnCo_2O_4$ nanocomposites.

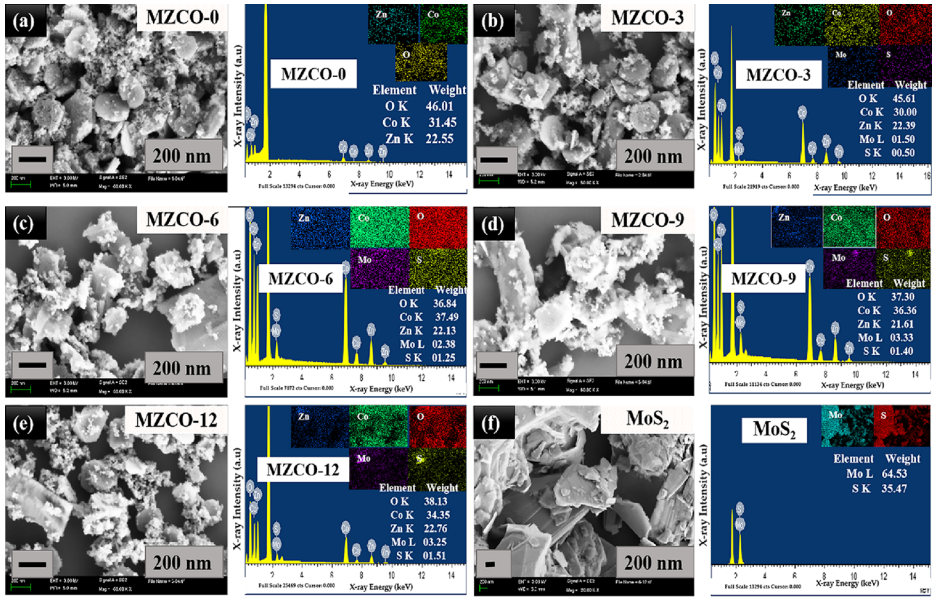

Figure 3. (a) SEM images and EDS spectra (inside mappings of element) of MZCO-0, (b) MZCO-3, (c) MZCO-6, (d) MZCO-9, (e) MZCO-12, and (f) MoS_2.

2.3. Fabrication of a Sensor. The gas sensor was fabricated using a thin film, and fabrication method was related to the literature;[8] the thin film is exposed in Figure 1. When the autoclave process was completed, the mixture was washed with ethanol and DI by centrifugation to remove impurities; after that, the final solution was coated on an alumina substrate with one pair of Ag intermediate electrodes by using the spin coating method. The ceramic sensor chip was fixed on the spin coating machine, the suspension liquid in the test tube was shaken evenly, a small amount of the suspension liquid was drawn with a disposable dropper, and 4−5 drops were dropped on the side of the ceramic negative with a cross-fingered electrode to spin coat into a film. After that, the coated sensor sheet was placed into a glass dish and placed in an oven at 130 °C for 10 min. The purpose was to volatilize the alcohol and dry the sensor sheet. After drying twice, the dried sensor sheet was put into a crucible and placed in a muffle furnace for sintering. The temperature was 300 °C, the duration was 2 h, the heating rate was 2 °C/min, and it naturally cooled to room temperature to obtain the heterostructure thin film sensor sheet for detecting different gases in this paper. $ZnCo_2O_4$ is a p-type material, but in our experiments, it showed n-type behavior because of the electron−hole movements, and the highest response toward H_2S toxic gas was studied. The response was calculated, such as the ratio of thin film resistance in air (R_a) to the resistance in gas (R_g) ($S = R_a/R_g$).

2.4. Physical Characterization of Materials. The microstructural properties and morphologies of the synthesized products were observed by XRD (D/MAX-Ultima, Cu Kα source, 2°/min scanning rate and the scanning angle from 10° to 80° as well as the power was 40 kV and 40 mA, Rigaku, Tokyo, Japan), SEM (ZEISS Gemini 500, Carl Zeiss AG, Oberkochen, Germany) with the component of EDS, TEM (JEM-3200FS, JEOL, Tokyo, Japan), and HRTEM (JEM-2100F, JEOL). In addition, XPS and BET analysis were carried out using ESCALAB 250XI (Thermo Fisher Scientific, Waltham, MA, USA) and ASAP2010C instrument (Norcross GA, USA), respectively.

https://doi.org/10.1021/acsomega.3c06876
ACS Omega 2023, 8, 47023−47033

3. EXPERIMENTAL RESULTS AND DISCUSSION

3.1. Morphology and Structure. The crystalline nature of the synthesized products was observed using XRD diffraction peaks, as exposed in Figure 2a,b. The diffraction peaks observed from the patterns corresponded to the crystallographic standard database files of MoS_2 and $ZnCo_2O_4$. The XRD diffraction patterns of all the samples showed the diffraction peaks of $ZnCo_2O_4$ at the 2θ values of 31.21°, 36.80°, 44.73°, 59.28°, and 65.14° corresponding to (220), (311), (400), (511), and (440) planes of $ZnCo_2O_4$ (JCPDS No. 23-1390), respectively. Except for the diffraction peaks of MZCO-0, a highly strong height of the MoS_2 peak was observed in all other nanocomposites at the 2θ value of 14.37° matched with the (002) plane of MoS_2 (JCPDS No. 37-1492). No extra peaks were found in all patterns, suggesting that the samples were well-ordered and possessed good crystallinity and clarity. Besides, estimated crystallite sizes of $ZnCo_2O_4$ cubes in all nanocomposites were calculated using the Debye−Scherrer formula, such as 10.59, 11.82, 9.36, 12.86, and 15.07 nm based on the (311) peaks, while 10.02, 12.23, 11.98, 13.06, and 14.39 nm based on (440) peaks in the nanocomposites of MZCO-0, MZCO-3, MZCO-6, MZCO-9, and MZCO-12, respectively. It was found that adding the contents of MoS_2 in the nanocomposites increased the crystallite size of $ZnCo_2O_4$.

Figure 3 revealed the SEM images of all of the nanocomposites. The cube-shaped $ZnCo_2O_4$ nanoparticles with an average particle size of 30−40 nm were seen from the SEM images of MZCO-0, besides the uniform scattering of all the elements present in MZCO-0 and EDS spectrum were noticed in Figure 3a. The SEM images and EDS spectrum (each element scattering) of the nanocomposites (MZCO-*P*, *P* = 3, 6, 9, and 12) shown in Figure 3b−e clearly observed the modification of cube-shaped $ZnCo_2O_4$ nanoparticles onto the stacks structure of MoS_2. Figure 3f shows the SEM image of MoS_2, which is very clear about the stacks structure. From SEM images, first of all, the morphology of MoS_2 and $ZnCo_2O_4$ was observed; second, it was noticed that the particle size of $ZnCo_2O_4$ was enhanced by adding MoS_2 contents in the nanocomposites. SEM results corresponded to XRD results, in which it was stated that by adding MoS_2 to the samples, the crystallite sizes of $ZnCo_2O_4$ were improved.

The decoration of cube-shaped $ZnCo_2O_4$ with the stacks structure of MoS_2 was further verified by TEM and HRTEM images. In Figure 4a, TEM images of MZCO-0 were disclosed, which showed the average particle size (30−40 nm) of cube-shaped $ZnCo_2O_4$ nanoparticles; in particular, the clear lattice fringes with a lattice spacing of 0.246 corresponded to the (311) plane of spinel $ZnCo_2O_4$. Also, in Figure 4b−e, TEM images proved the stacks structure of MoS_2 and cube-shaped $ZnCo_2O_4$ nanoparticles were checked, and HRTEM images exposed lattice spacings of 0.62 and 0.246 related to the (002) and (311) planes of MoS_2 and $ZnCo_2O_4$, respectively. In Figure 4f, clear lattice spacing (0.62) and stack structure of MoS_2 were verified. TEM and HRTEM evidenced that the particle sizes of $ZnCo_2O_4$ (30−40 nm) were detected. Gradually, their size was enhanced by adding MoS_2 contents in the nanocomposite, corresponding to the XRD results.

In Figure 5, the nitrogen adsorption−desorption isotherms were performed for the nanocomposites of MZCO-0, MZCO-3, MZCO-6, MZCO-9, MZCO-12, and MoS_2 to interpret their porosity and distribution. In the inset of images Figure 5a−f,

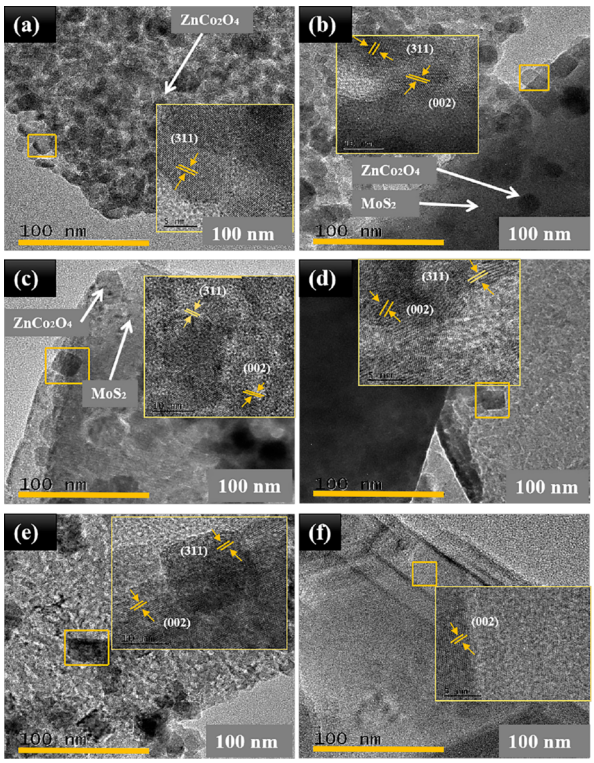

Figure 4. TEM images and HRTEM images of (a) MZCO-0, (b) MZCO-3, (c) MZCO-6, (d) MZCO-9, (e) MZCO-12, and (f) MoS_2.

the pore size distribution diagrams were exposed, suggesting that all the nanocomposites have an obvious hysteresis loop, which verified the presence of many pores. The pore size distribution diagrams have also concluded that the main peaks were found in the range of 1−20 nm, signifying nanocomposites' mesoporous structure.[24] It was found that pore volumes of MZCO-0, MZCO-3, MZCO-6, MZCO-9, MZCO-12, and MoS_2 were 0.1822, 0.2223, 0.1804, 0.1692, 0.2271, and 0.1563 cm^3/g, respectively. Besides, nitrogen adsorption−desorption isotherms were carried out at the specific surface area of all of the nanocomposites. BET surface areas of nanocomposites of MZCO-0, MZCO-3, MZCO-6, MZCO-9, MZCO-12, and MoS_2 in Figure 5a−f were 31.08, 33.14, 37.01, 38.41, 44.08, and 26.41 m^2/g, respectively. Due to the higher BET surface areas and wide pore size distributions of nanocomposite MZCO-6 compared with MZCO-0, the gas sensor of MZCO-6 detected a high response toward 10 ppm of H_2S.

The surface chemical composition and electronic state of the nanocomposites of MZCO-0 and MZCO-6 were measured using X-ray photoelectron spectra characteristics. The details were as follows: in Figure 6a, the full scan spectra were given, which specified the presence of all the elements such as M, S, Zn, Co and O in the MZCO-6 nanocomposite. Next, the high-resolution spectra of Zn 2p are displayed in Figure 6b,c. The peaks in the spectra of MZCO-6 (a) and MZCO-0 (b) corresponded to Zn $2p_{3/2}$ and Zn $2p_{1/2}$ (1021.3 and 1044.4 eV),[25] and the binding energy values were the same in both the materials but the peak intensities in the spectrum of MZCO-6 were higher than MZCO-0. After that, the spectra of Co 2p exposed in Figure 6d,e studied the peak intensities difference and chemical shift in the binding energies. Two main peaks of Co $2p_{3/2}$ and Co $2p_{1/2}$ were related to 795.1 and 780.1 eV in

https://doi.org/10.1021/acsomega.3c06876
ACS Omega 2023, 8, 47023−47033

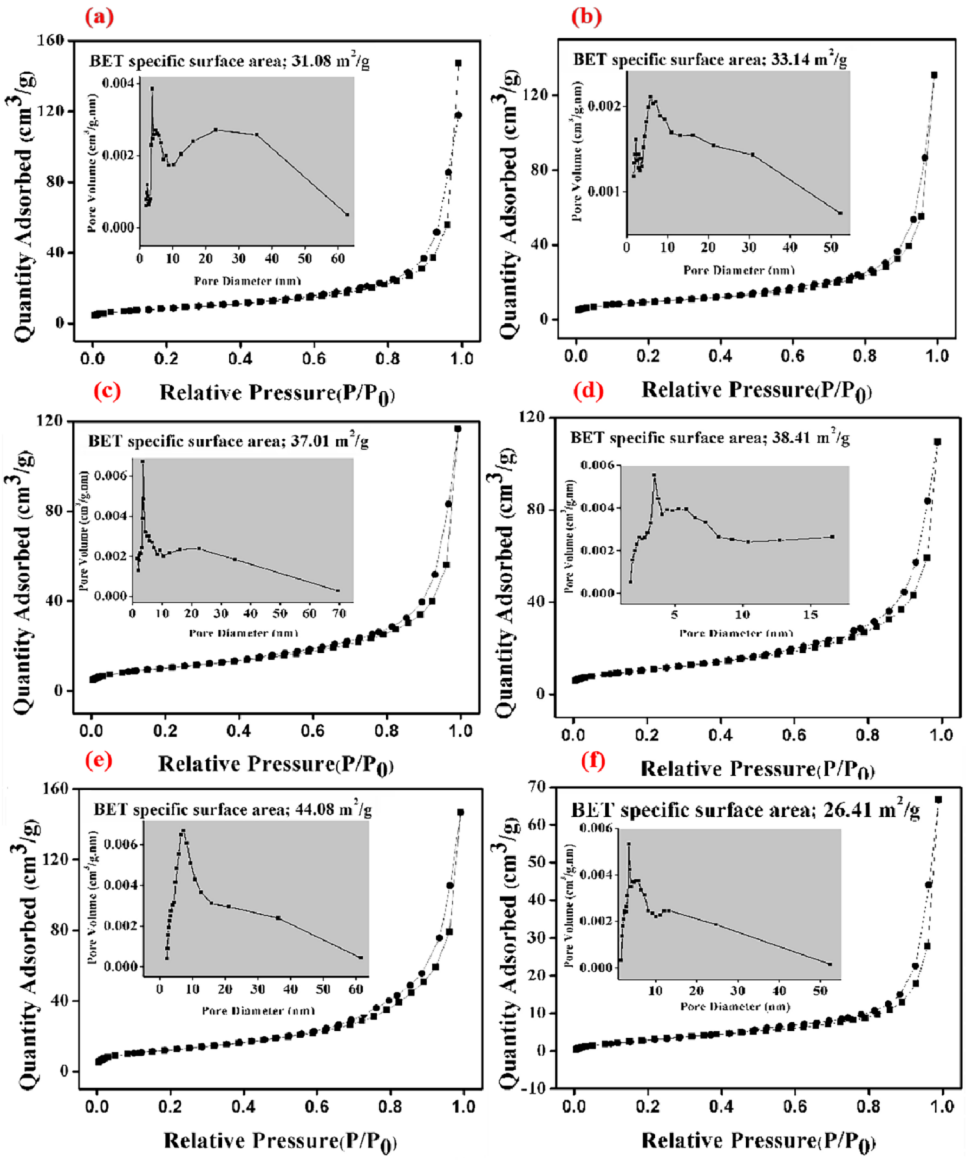

Figure 5. N_2 adsorption−desorption isotherms and pore size distributions of MZCO-0 (a), MZCO-3 (b), MZCO-6 (c), MZCO-9 (d), MZCO-12 (e), and MoS_2 (f).

the spectrum of MZCO-6, while $2p_{3/2}$ and Co $2p_{1/2}$ in the spectrum of MZCO-6 were related to 795.2 and 780.2 eV, which informed the valence state of Co^{2+},[26] also the peak intensities were higher in MZCO-6 than MZCO-0. Besides these two peaks, there were two satellite peaks in both nanocomposites at the peak values of (789.8, 805.5, 790.2, and 804.9). O 1s spectra in Figure 6f,g revealed two peaks in both the nanocomposites of MZCO-6 and MZCO-0 at the values of 529.8, 531.5 eV and 529.7, 531.7 eV, and these peaks were related to two oxygen states such as the crystal lattice (Olatt) and chemisorbed oxygen specie (Oads), respectively.[27] In Figure 6h, Mo 3d spectra of MZCO-6 were displayed, and three peaks at 229.5, 232.4, and 235.4 eV were related to Mo^{4+} $3d_{5/2}$, Mo^{4+} $3d_{3/2}$, and Mo^{6+} $3d_{5/2}$.[28,29] Finally, in Figure 6i, the S 2p spectra of MZCO-6 showed two peaks of S $2p_{3/2}$ and S $2p_{1/2}$.[30,31]

3.2. Gas Sensing Performance. The dynamic response transients of MZCO-6 toward various H_2S concentrations are shown in Figure 7a. The res./rec. times for 10, 5, 3, 1, and 0.5 ppm were 12/28, 13/40, 10/30, 7/29, and 9/27 s, respectively. Besides, the sensor exposed the response to 0.5 ppm of H_2S, and the response was 1.2. In order to spotlight the res./rec. speed toward 10 ppm of H_2S, we have placed a graph between resistance and res./rec. time in Figure 7b, which showed that when the sensor was in a H_2S atmosphere, the curve went down (res. time, 12 s) and around (4×10^5) it was in the stable state, then in air atmosphere, it started to go back (rec. time, 28 s) to the original state. In Figure 7c, the res./rec. times of MZCO-6 toward C_4H_{10}, H_2, and NO_2 were exposed, which stated that the response times were 11, 15, and 18 s, and recovery times were 26, 40, and 22 for C_4H_{10}, H_2, and NO_2, respectively. The linear relation between the response and H_2S parts per million is crucial because linearity can make a sensor a promising candidate in gas sensors. Figure 7d exposed that the responses of the sensor (MZCO-6) were 6.6, 4, 3.4, 1.8, and 1.2 toward 10, 5, 3, 1, and 0.1 ppm, respectively, while fitting curve values were 6.7, 4.5, 3.35, 1.778, and 1.18 based on the equation of $Y = 1.7735 \times 0.5824$, and regression coefficient, R^2, 0.9899. It was clear from the figure with the increasing H_2S concentrations, the response was gradually

https://doi.org/10.1021/acsomega.3c06876
ACS Omega 2023, 8, 47023−47033

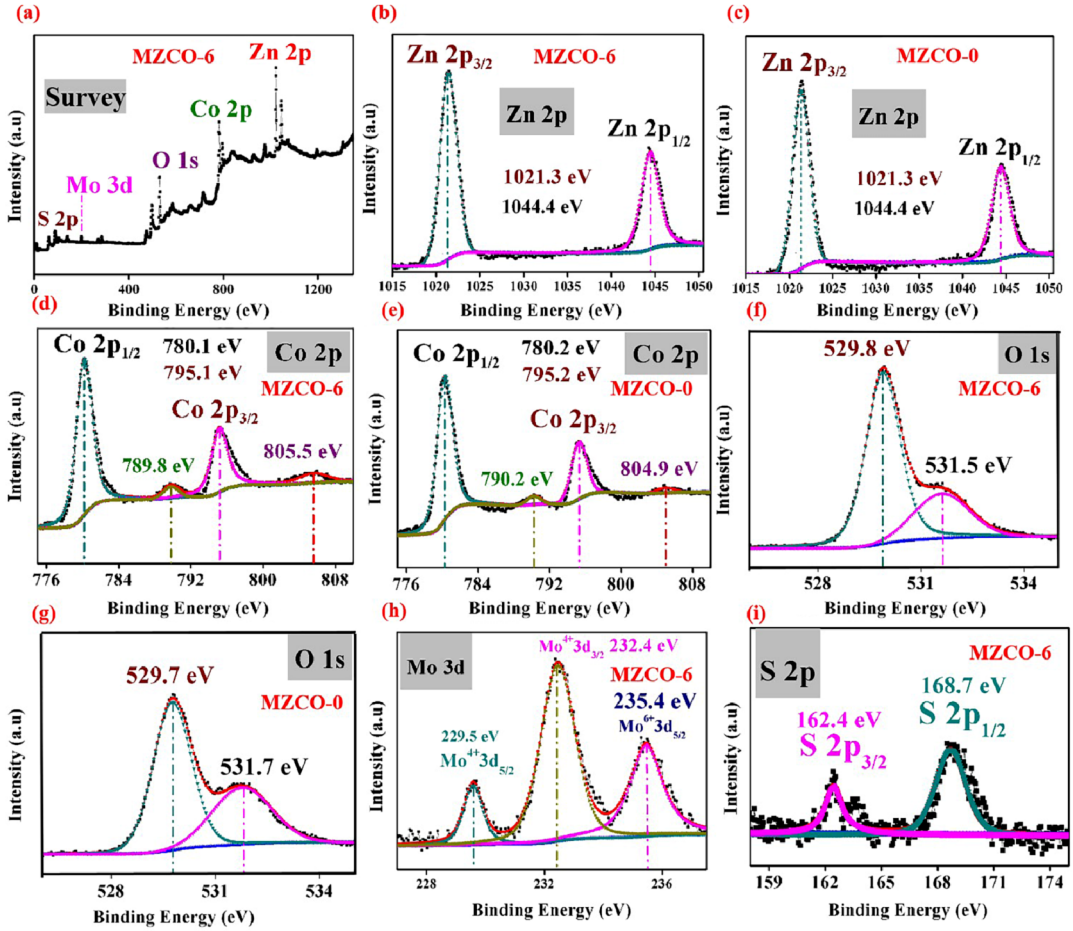

Figure 6. XPS spectra of (a) full survey of MZCO-6, (b) Zn 2p spectrum of MZCO-6, (c) Zn 2p spectrum of MZCO-0, (d) Co 2p spectrum of MZCO-6, (e) Co 2p spectrum of MZCO-0, (f) O 1s spectrum of MZCO-6, (g) O 1s spectrum of MZCO-0, (h) Mo 3d spectrum of MZCO-6, and (i) S 2p spectrum of MZCO-6.

increased, suggesting its linearity between the response and H_2S concentrations.

Figure 8a studied the gas sensing properties of MoS_2, MZCO-0, MZCO-3, MZCO-9, and MZCO-12 to 10 ppm of H_2S at RT. The responses to MoS_2, MZCO-0, MZCO-3, MZCO-9, and MZCO-12 were 2.5, 1.2, 2.15, 6.6, 2, and 1.7, respectively. Selectivity is an essential parameter for a gas sensor. In our case, the selectivity of MZCO-*P*, *P* = 0, 3, 6, 9, and 12 based gas sensors was measured in Figure 8b, and the selectivity was checked out using four toxic gases,namely, H_2S, C_4H_{10}, H_2, and NO_2 (10 ppm) at RT. The sensor based on MZCO-6 detected the response of 6.6, 2.0, 1.9, and 2.1 toward H_2S, C_4H_{10}, H_2, and NO_2, respectively. These results indicated that the selectivity of MZCO-6 was calculated as the ratio of the highest response toward H_2S and the second highest response toward NO_2 (selectivity = $S_{10\ ppm\ of\ H_2S}/S_{10\ ppm\ of\ NO_2}$), and then its calculated selectivity was around 3.14. The selectivity results stated that the response of MZCO-6-based gas sensors toward 10 ppm of H_2S was almost three times higher than other checked gases, which pointed out that the sensor exposed a high response and impressive selectivity toward H_2S. In Table 1, some sensors were reported against our sensor, which suggested that the current sensor exposed high response (6.6), short response/recovery times (12/28 s), good stability (28 days), better reproducibility (5 cycles), good selectivity (3.14), and linear relationship between response and H_2S concentration, and the above features revealed that the simple fabricated sensor through our experiments is a potential candidate for real-time applications.

As far as we know, long-term stability and reproducibility are also imperative for gas sensors. Herein, Figure 9 examined the stability test for all nanocomposites MZCO-*P*, *P* = 0, 3, 6, 9, and 12 based gas sensors, which showed that the sensors were stable for 28 days. There was no obvious fluctuation in the response with passage of time, exhibiting its adequate stability for detecting H_2S at RT. The most stable sensor was the MZCO-6-based sensor among all other tested sensors.

To detect the low concentrations of gases at RT, high selectivity and good reproducibility are great challenges for a sensor to prove its promising applicability in applications. Considering the above factors, reproducibility is also very important. Figure 10a shows the five cycles of gas-sensing performance of MZCO-6. As clear from the figure, the resistance in the gas and air atmosphere was almost the same in five cycles; after every cycle, the resistance can go down in the H_2S atmosphere and back into the air atmosphere, suggesting good reproducibility and reversibility of the current sensor. Figure 10b exposes the graph between the response of a sensor based on the MZCO-6 nanocomposite and various relative humidities (RH). The sensor was tested at RT, and the response was decreased a little at RH values of 45, 65, and 85,

https://doi.org/10.1021/acsomega.3c06876
ACS Omega 2023, 8, 47023−47033

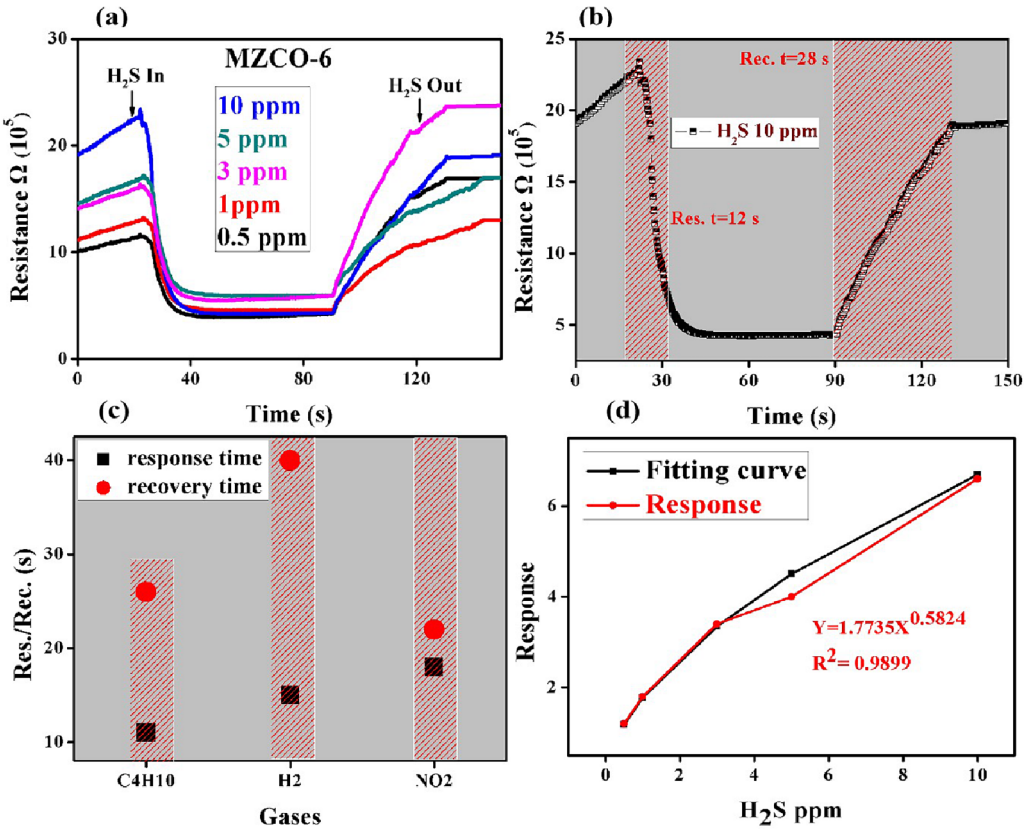

Figure 7. (a) Dynamic res./rec. curve and resistance of MZCO-6 to 10−0.5 ppm of H_2S at RT, (b) resistance change of the MZCO-6 composite-based sensor to 10 ppm of H_2S, (c) the plots of response/recovery times toward 10 ppm of C_4H_{10}, H_2, and NO_2 of MZCO-6, and (d) relation between response and different concentrations of H_2S of MZCO-6.

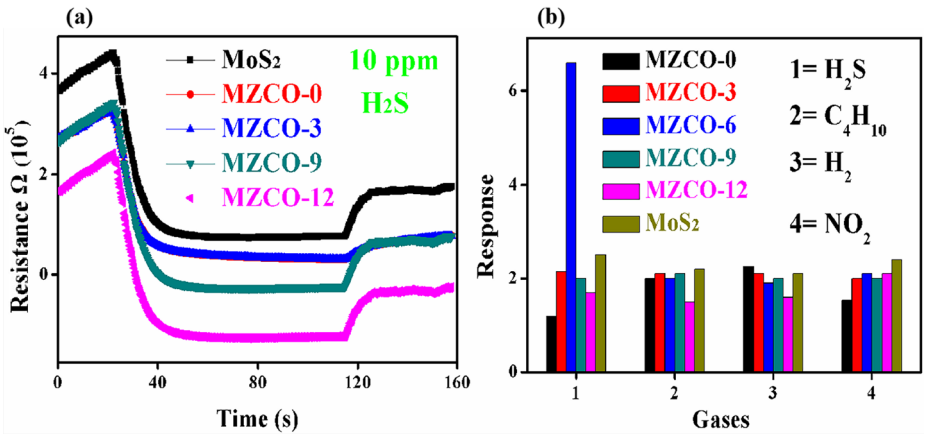

Figure 8. (a) Dynamic res./rec. curve and resistance of MoS2, MZCO-0, MZCO-3, MZCO-9, and MZCO-12 to 10 ppm of H_2S at RT and (b) selectivity test.

which verified that the sensor has impressive stability against humidity.

3.3. Gas-Sensing Mechanism. We have synthesized a series of nanocomposites based on stacks MoS_2 and cube-shaped $ZnCo_2O_4$ nanoparticles and applied them as gas sensors, and the highest response toward 10 ppm of H_2S was received. To understand the gas-sensing mechanism of nanocomposites, this may achieve great attention for RT H_2S detection. In general, the gas-sensing mechanism is based on the variation in resistance in air and gas environments; however, the resistance changes based on the charge carrier concentration of the material surface. In Figure 11, the gas-sensing mechanism and band diagram are described to prove the sensing mechanism. In our experiments, as we can see, the main sample MZCO-6 exposed the highest response toward 10 ppm of H_2S compared with other tested sensors. The highest response may be correlated to some factors explained as follows: first of all, a p−n heterojunction formed between the n-type stacks MoS_2 and p-type $ZnCo_2O_4$, which provides the large quantity of electron transfer in the nanostructures; second, the stacks structure, which can facilitate the rapid diffusion and electrons transmission density (SEM); third, the stacks structure of MoS_2 enhanced the BET surface area of the nanocomposites, which can be considered one of the

https://doi.org/10.1021/acsomega.3c06876
ACS Omega 2023, 8, 47023−47033

Table 1. Comparison of Various Gas Sensors[a]

materials	operating temp. (°C)	res./rec. time	response (gas ppm)	LOD	stability	ref.
PANI/MoS_2/ SnO_2	RT	21 s/130 s	10.9 (NH_3, 100 ppm)	200 ppb		36
SnO_2 /MoS_2	RT	6.8 min/2.7 min	− (NO_2, 10 ppm)			37
MoS_2	130	1.4 s/2.9 s	86.9 (HCHO, 100 ppm)	10 ppm	30 days	38
$ZnCo_2O_4$	90	−/104 s	6.39 (H_2S, 10 ppm)	50 ppb		39
ZnO	500	1080 s/300 s	35 (H_2S, 50 ppm)			40
ZnO:Pd	300	720 s/36000 s	∼1900 (H_2S, 500 ppm)			41
CuO/SWCNTs	150		6 (H_2S, 0.1 ppm)	0.1 ppm		42
Pt-doped α-Fe_2O_3	200		60 (acetone, 1000 ppm)			43
SnO_2−ZnO	360	5 s/1 s	17 (ethanol, 2500 ppm)			44
$NiCo_2O_4$@SnO_2	160		8.87 (ethanol, 100 ppm)	2 ppm	30 days	45
MoS_2 -$ZnCo_2O_4$	RT	12 s/28 s	6.6 (H_2S, 10 ppm)	0.5 ppm	28 days	this work

[a]Temp. = temperature; Res./Rec. = response/recovery; ref. = references.

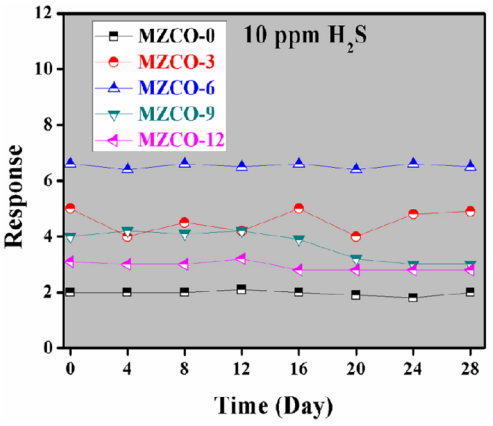

Figure 9. Stability test for all sensors at RT.

imperative factors to enhance the gas sensing properties such as high response, good selectivity, and short response/recovery times, toward H_2S (BET); fourth, moreover, as XPS approved it, the more oxygen species can be adsorbed on the surface of the sensing material, which may help out to increase the resistance. Besides, the interaction between 2D stacks materials is much smaller than the interionic forces, and the interlayer forces are regulated by the surface charge distribution.[32] Therefore, the use of stack 2D materials can reduce the surface potential (reduce the barrier resistance), which greatly improves the resolution and response of the sensor.

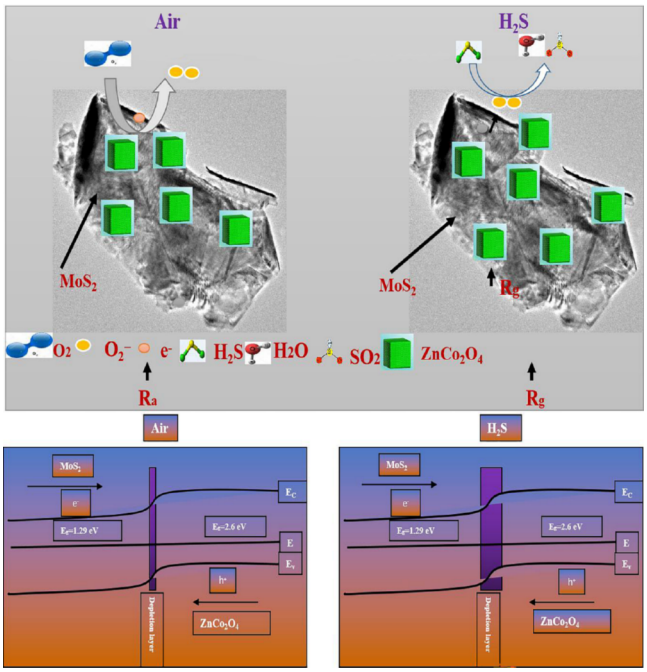

Figure 11. Gas-sensing mechanism and energy band gap structure of the MZCO-6 based gas sensor at RT toward 10 ppm of H_2S.

The band gaps of both materials played a very crucial role in the sensing mechanism; the band gaps of MoS_2 (1.29) and

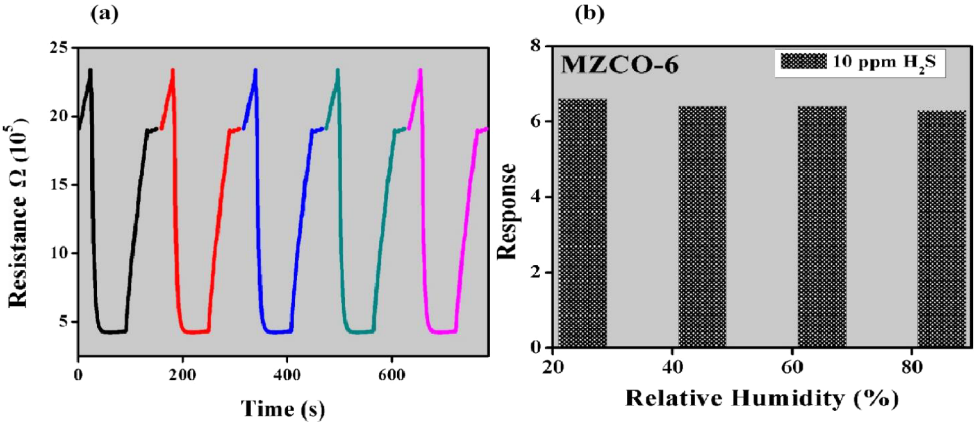

Figure 10. (a) The reproducibility of MZCO-6-based gas sensor at RT toward 10 ppm of H_2S and (b) the response vs different RH at RT toward 10 ppm of H_2S.

https://doi.org/10.1021/acsomega.3c06876
ACS Omega 2023, 8, 47023−47033

$ZnCo_2O_4$ (2.6) are shown in Figure 11. Besides, the work functions for MoS_2 and $ZnCo_2O_4$ were 5.2−5.4 eV[33] and 5.22 eV,[34] respectively. It showed that after forming the p−n heterojunction between two materials, the electron will move from MoS_2 to $ZnCo_2O_4$ and holes in the opposite directions until an equilibrium state was formed, besides the p−n junction can reduce the conductivity of the nanocomposites in the air atmosphere, while enhanced the conductivity in H_2S atmosphere and vice versa in the form of resistance. The surface states and hydroxides of the stack materials introduce impurity levels into the band gap,[34,35] thereby enhancing the electron−hole recombination on the surface and resulting in an increased response.

Moreover, as shown in the diagram, when the sensor of MZCO-6 was in an air atmosphere, the oxygen molecules were adsorbed on the surface of the material and accepted electrons to convert them into O_2^- (adsorbed oxygen), besides making a hole accumulation layer (HAL) from the holes left on the surface. In air, oxygen adsorption causes the MoS_2 surface to gather positive space charge, its surface potential causes the barrier resistance to increase, and the reactions based on temperatures were exposed in eqs 1−4):

$$O_{2(gas)} \rightarrow O_{2(ads)} \quad (1)$$

$$O_{2(ads)} + e^- \rightarrow O^-_{2(ads)} \qquad T < 100\ ^\circ C \quad (2)$$

$$O^-_{2(ads)} + e^- \rightarrow 2O^-_{(ads)} \qquad 100\ ^\circ C \leq T \leq 300\ ^\circ C \quad (3)$$

$$O^-_{(ads)} + e^- \rightarrow O^{2-}_{(ads)} \qquad T > 300\ ^\circ C \quad (4)$$

After that, when the sensor of MZCO-6 was in H_2S atmosphere, the sensor, herein, $ZnCo_2O_4$ is a p-type semiconductor but it worked as an n-type sensor because of the holes and electrons movement. When the sensor was in the H_2S atmosphere, it reacted with O_2^- by forming SO_2 and H_2O as shown in eq 5); besides, there was an interaction between the H_2S gas and hydroxyl species of the thin film sensor as well. During the reaction, the electrons went back to the conduction band, and an unbalanced electric field reduced the barrier height. Consequently, the electron will move from MoS_2 to $ZnCo_2O_4$ and holes in the opposite directions, which in turn expand the HAL and decreased the resistance of the sensor in H_2S environment. Also, in H_2S gas, it can be seen from eq 5) that the surface potential decreases or disappears, resulting in a decrease in the barrier resistance

$$2H_2S\ (g) + 2O^-_2(ads) \rightarrow 2SO_2 + 2H_2O + 3e^- \quad (5)$$

4. CONCLUSION

In this study, we designed a new series of sensors based on the nanocomposite of stacks MoS_2 and cube-shaped $ZnCo_2O_4$; these nanocomposites were synthesized hydro-thermally. Various characterizations were performed, for example, XRD, SEM, EDS, TEM, HRTEM, BET, and XPS, to confirm the morphology and structural properties. From XRD, it was shown that the crystallite size was increased with the increase of MoS_2 contents in the nanocomposites, besides particle size also increased by adding MoS_2 contents (SEM and TEM). Furthermore, BET results proved that the nanocomposites have higher BET-specific surface areas than pure $ZnCo_2O_4$ and more oxygen adsorption of MZCO-6 than pure $ZnCo_2O_4$ verified by XPS. After that, the synthesized materials were tested as gas sensors, and the gas sensor (thin solid film) was fabricated through a mixture of solid and water. Various sensors based on nanocomposites (MZCO-*A*, *A* = 0, 3, 6, 9, 12) were used for detecting four kinds of toxic gases. The highest response toward 10 ppm of H_2S gas was detected by the gas sensor of MZCO-6 against all other tested sensors. The response was 6.6 for 10 ppm of H_2S. Besides the highest response, the sensor of MZCO-6 exposed good selectivity (3.14), better stability (28 days), minimum LOD (0.5 ppm), good reproducibility (5 cycles), and an almost linear relationship between response and concentrations of H_2S (0.5−10 ppm). The marvelous gas sensing properties of MZCO-6 were related to some crucial points such as p−n heterojunction, stack structure of MoS_2, higher BET surface area, and increased adsorption of oxygen species. RT H_2S gas sensors fabricated in simple ways are finding novel applications in daily routine activities. In this way, our synthesized nanocomposite-based gas sensor has promising applicability in gas sensors.

■ ASSOCIATED CONTENT

Data Availability Statement

The data sets generated during and/or analyzed during the current study are available from the corresponding author on reasonable request.

■ AUTHOR INFORMATION

Corresponding Authors

Hongpeng Zhang − *Marine Engineering College, Dalian Maritime University, Dalian 116026, China*; Email: zhppeter@dlmu.edu.cn

Daru Chen − *Hangzhou Institute of Advanced Studies, Zhejiang Normal University, Hangzhou 311231, China*; Phone: Tel.: + 86 411 84729934; Email: daru@zjnu.cn

Ali Akhtar − *Hangzhou Institute of Advanced Studies, Zhejiang Normal University, Hangzhou 311231, China*; orcid.org/0000-0002-3674-877X; Email: aliakhtar6091995@gmail.com

Author

Shama Sadaf − *Marine Engineering College, Dalian Maritime University, Dalian 116026, China*

Complete contact information is available at: https://pubs.acs.org/10.1021/acsomega.3c06876

Author Contributions

All authors contributed to the study conception and design. Material preparation, data collection, and analysis were performed by S.S. and A.A. The first draft of the manuscript was written by S.S. and A.A. and H.Z. helped in revising the manuscript. All authors read and approved the final manuscript.

Notes

The authors declare no competing financial interest.

■ ACKNOWLEDGMENTS

This work was supported by the National Natural Science Foundation of China (no. 51679022), the Natural Science Foundation of China (no. 52271303), the Dalian Science Technology Innovation Fund (no. 2019J12GX023), the Liaoning Revitalization Talents Program (no. XLYC2002074), Fundamental Research Funds for the Central Universities (no. 3132022219), Fundamental Research Funds

for the Central Universities (no. 3132021501), the Technology Innovation Foundation of Dalian (no. 2022JJ11CG010), and "the Pioneer" and "Leading Goose" R&D Program of Zhejiang, grant no. 2022C03084.

REFERENCES

(1) Shirsat, M. D.; Bangar, M. A.; Deshusses, M. A.; Myung, N. V.; Mulchandani, A. Polyaniline nanowires-gold nanoparticles hybrid network based chemiresistive hydrogen sulfide gas sensor. *Appl. Phys. Lett.* **2009**, *94*, 083502.
(2) Ramgir, N. S.; Sharma, P. K.; Datta, N.; Kaur, M.; Debnath, A. K.; Aswal, D. K.; Gupta, S. K. Room temperature H_2S gas sensor based on Au modified ZnO nanowires. *Sens. Actuators, B* **2013**, *186*, 718−726.
(3) Wang, Y.; Liu, F.; Yang, Q.; Gao, Y.; Sun, P.; Zhang, T.; Lu, G. Mesoporous $ZnFe_2O_4$ prepared through hard template and its acetone sensing properties. *Mater. Lett.* **2016**, *183*, 378−381.
(4) Li, C.; Choi, P. G.; Kim, K.; Masuda, Y. High performance acetone gas sensor based on ultrathin porous NiO nanosheet. *Sens. Actuators, B* **2022**, *367*, 132143.
(5) Chaloeipote, G.; Prathumwan, R.; Subannajui, K.; Wisitsoraat, A.; Wongchoosuk, C. 3D printed CuO semiconducting gas sensor for ammonia detection at room temperature. *Mater. Sci. Semicond. Process.* **2021**, *123*, 105546.
(6) Joshi, N.; da Silva, L. F.; Jadhav, H.; M'Peko, J.-C.; Torres, B. B. M.; Aguir, K.; Mastelaro, V. R.; Oliveira, O. N., Jr. One-step approach for preparing ozone gas sensors based on hierarchical $NiCo_2O_4$ structures. *RSC Adv.* **2016**, *6*, 92655−92662.
(7) Xiong, Y.; Zhu, Z.; Ding, D.; Lu, W.; Xue, Q. Multi-shelled $ZnCo_2O_4$ yolk-shell spheres for high-performance acetone gas sensor. *Appl. Surf. Sci.* **2018**, *443*, 114−121.
(8) Liu, J.; Lv, J.; Shi, J.; Wu, L.; Su, N.; Fu, C.; Zhang, Q. Size effects of tin oxide quantum dot gas sensors: from partial depletion to volume depletion. *J. Mater. Res. Technol.* **2020**, *9*, 16399−16409.
(9) Xu, T.; Zhang, M.; Zhao, F.; Zhao, J.; Cong, W.; Xie, C.; Yang, Z.; Wang, G.; Li, J. Highly sensitive detection of H_2S gas at low temperature based on $ZnCo_2O_4$ microtube sensors. *J. Hazard. Mater.* **2022**, *440*, 129753.
(10) Li, X.; Zhang, Y.; Cheng, Y.; Tan, W. MOF-derived porous hierarchical $ZnCo_2O_4$ micro-flowers for enhanced performance gas sensor. *Ceram. Int.* **2021**, *47*, 9214−9224.
(11) Ebrahimi, M.; Soleimanian, V.; Ghasemi, M.; Nekoeinia, M.; Mokhtari, A. Effects of graphene quantum dots on microstructure, optical and gas sensing properties of coral-like $ZnCo_2O_4$ nanoparticles. *Phys. B* **2023**, *650*, 414439.
(12) Liu, M. M.; Ma, S.Y.; Cai, Y. H.; Ma, N. N.; Wang, L.; Sheng, H. $ZnO/ZnCo_2O_4$ composite prepared by one-step hydrothermal method for high-performance ethylene glycol sensor. *Ceram. Int.* **2022**, *48*, 22305−22312.
(13) Zhou, T.; Sui, N.; Zhang, R.; Zhang, T. Cabbage-shaped zinc-cobalt oxide ($ZnCo_2O_4$) sensing materials: Effects of zinc ion substitution and enhanced formaldehyde sensing properties. *J. Colloid Interface Sci.* **2019**, *537*, 520−527.
(14) Li, J.; Yu, K.; Tan, Y.; Fu, H.; Zhang, Q.; Cong, W.; Song, C.; Yin, H.; Zhu, Z. Facile synthesis of novel $MoS_2@SnO_2$ heteronanoflflowers and enhanced photo-catalysis and field-emission properties. *Dalton Trans.* **2014**, *43*, 13136−13144.
(15) Chen, L.; Arshad, M.; Chuang, Y.; Nguyen, T.-B.; Wu, C.-H.; Chen, C.-W.; Dong, C.-D. A novel nano-heterojunction MoS_2/α-Fe_2O_3 photocatalysts with high photocatalytic and photoelectrochemical performance under visible light irradiation. *J. Alloys Compd.* **2023**, *947*, 169577.
(16) Mohan, M.; Shetti, N. P.; Aminabhavi, T. M. Phase dependent performance of MoS_2 for supercapacitor applications. *J. Energy Storage* **2023**, *58*, 106321.
(17) HE, H.-b.; LIU, Z.; PENG, C.-q.; LIU, J.; WANG, X.-f.; ZENG, J. 3D MoS_2/graphene nanoflowers as anode for advanced lithium-ion batteries. *Trans. Nonferrous Met. Soc. China* **2022**, *32*, 4041−4049.
(18) Li, Y.; Song, X.; Li, L.; Wu, W.; Tao, K.; Ying, Z.; Hu, Y.; Zhou, Y.; Zhang, R.; Wang, G.; Wen, F. Low concentration CO gas sensor constructed from MoS_2 nanosheets dispersed SnO_2 nanoparticles at room temperature under UV light. *Ceram. Int.* **2023**, *49*, 10249−10254.
(19) Bai, H.; Guo, H.; Feng, C.; Wang, J.; Liu, B.; Xie, Z.; Guo, F.; Chen, D.; Zhang, R.; Zheng, Y. Light-activated ultrasensitive NO_2 gas sensor based on heterojunctions of CuO nanospheres/MoS_2 nanosheets at room temperature. *Sens. Actuators, B* **2022**, *368*, 132131.
(20) Kumar, R. R.; Murugesan, T.; Dash, A.; Hsu, C.-H.; Gupta, S.; Manikandan, A.; Anbalagan, A. k.; Lee, C.-H.; Tai, N.-H.; Chueh, Y.-L.; Lina, H.-N. Ultrasensitive and light-activated NO_2 gas sensor based on networked MoS_2/ZnO nanohybrid with adsorption/desorption kinetics study. *Appl. Surf. Sci.* **2021**, *536*, 147933.
(21) Hu, J.; Liu, X.; Zhang, J.; Gu, X.; Zhang, Y. Plasmon-activated NO_2 sensor based on Au@MoS_2 core-shell nanoparticles with heightened sensitivity and full recoverability. *Sens. Actuators, B* **2023**, *382*, 133505.
(22) Wu, D.; Akhtar, A. Ppb-Level Hydrogen Sulfide Gas Sensor Based on the Nanocomposite of MoS_2 Octahedron/ZnO-Zn_2SnO_4 Nanoparticles. *Molecules* **2023**, *28*, 3230.
(23) Duong, T. T. H.; Hau, H. H.; Hong, L. T.; Vu, L. A.; Hung, C. M.; Van Duy, N.; Van Hieu, N.; Hoa, N. D. PtO_2-decorated MoS_2 ultrathin nanostructures for enhanced NH_3 gas sensing properties, Mater. *Mater. Sci. Semicond. Process* **2022**, *151*, 106990.
(24) BoopathiRaja, R.; Parthibavarman, M.; Begum, A. N. Hydrothermal induced novel $CuCo_2O_4$ electrode for high performance super-capacitor applications. *Vacuum* **2019**, *165*, 96−104.
(25) Xie, Q.; Zeng, D.; Ma, Y.; Lin, L.; Wang, L.; Peng, D.-L. Synthesis of ZnO-$ZnCo_2O_4$ hybrid hollow microspheres with excellent lithium storage properties. *Electrochim. Acta* **2015**, *169*, 283−290.
(26) Zhang, N.; Lu, Y.; Fan, Y.; Zhou, J.; Li, X.; Adimi, S.; Liu, C.; Ruan, S. Metal−organic framework-derived $ZnO/ZnCo_2O_4$ microspheres modifified by catalytic PdO nanoparticles for sub-ppm-level formaldehyde detection. *Sens. Actuators, B* **2020**, *315*, 128118.
(27) Xiong, Y.; Xue, Q.; Ling, C.; Lu, W.; Ding, D.; Zhu, L.; Li, X. Effective CO_2 detection based on LaOCl-doped SnO_2 nanofibers: insight into the role of oxygen in carrier gas. *Sens. Actuators, B* **2017**, *241*, 725−734.
(28) Zhou, W.; Yin, Z.; Du, Y.; Huang, X.; Zeng, Z.; Fan, Z.; Liu, H.; Wang, J.; Zhang, H. Synthesis of few-layer MoS_2 nanosheet-coated TiO_2 nanobelt heterostructures for enhanced photocatalytic activities. *Small* **2013**, *9*, 140−147.
(29) Zhao, P. X.; Tang, Y.; Mao, J.; Chen, Y. X.; Song, H.; Wang, J. W.; Song, Y.; Zhang, X. M.; Liang, Y. Q. One-dimensional MoS_2-decorated TiO_2 nanotube gas sensors for efficient alcohol sensing. *J. Alloys Compd.* **2016**, *674*, 252−258.
(30) Cui, S.; Wen, Z.; Huang, X.; Chang, J.; Chen, J. Stabilizing MoS_2 nanosheets through SnO_2 nanocrystal decoration for high-performance gas sensing in air. *Small* **2015**, *11*, 2305−2313.
(31) Manuraj, M.; Chacko, J.; Unni, K. N. N.; Rakhi, R. B. Heterostructured MoS_2-RuO_2 nanocomposite: A promising electrode material for super capacitors. *J. Alloys Compd.* **2020**, *836*, 155420.
(32) Kong, S.-S.; Liu, W.-K.; Yu, X.-X.; Li, Y.-L.; Yang, L.-Z.; Ma, Y.; Fang, X.-Y. Interlayer interaction mechanism and its regulation on optical properties of bilayer SiCNSs. *Front. Phys.* **2023**, *18*, 43302.
(33) He, L.; Lv, H.; Ma, L.; Li, W.; Si, J.; Ikram, M.; Ullah, M.; Wu, H.; Wang, R.; Shi, K. Controllable synthesis of intercalated g-Bi_2MoO_6/graphene nanosheets composites for high performance NO_2 gas sensor at room temperature. *Carbon* **2020**, *157*, 22−32.
(34) Zhou, T.; Liu, X.; Zhang, R.; Wang, Y.; Zhang, T. NiO/$NiCo_2O_4$ truncated nanocages with PdO catalyst functionalization as sensing layers for acetone detection. *ACS Appl. Mater. Interfaces* **2018**, *10*, 37242−37250.
(35) Jia, Y.-H.; Gong, P.; Li, S.-L.; Ma, W.-D.; Fang, X.-Y.; Yang, Y.-Y.; Cao, M.-S. Effects of hydroxyl groups and hydrogen passivation on the structure, electrical and optical properties of silicon carbide nanowires. *Phys. Lett. A* **2020**, *384*, 126106.

https://doi.org/10.1021/acsomega.3c06876
ACS Omega 2023, 8, 47023−47033

(36) Liu, A.; Lv, S.; Jiang, L.; Liu, F.; Zhao, L.; Wang, J.; Hu, X.; Yang, Z.; He, J.; Wang, C.; Yan, X.; Sun, P.; Shimanoe, K.; Lu, G. The gas sensor utilizing polyaniline/MoS_2 nanosheets/SnO_2 nanotubes for the room temperature detection of ammonia. *Sens. Actuators, B* **2021**, *332*, 129444.
(37) Cui, S.; Wen, Z.; Huang, X.; Chang, J.; Chen, J. Stabilizing MoS_2 Nanosheets through SnO_2 Nanocrystal Decoration for High-Performance Gas Sensing in Air. *Small* **2015**, *11*, 2305−2313.
(38) Choi, G. J.; Mishra, R. K.; Gwag, J. S. 2D layered MoS_2 based gas sensor for indoor pollutant formaldehyde gas sensing applications. *Mater. Lett.* **2020**, *264*, 127385.
(39) Xu, T.; Zhang, M.; Zhao, F.; Zhao, J.; Cong, W.; Xie, C.; Yang, Z.; Wang, G.; Li, J. Highly sensitive detection of H_2S gas at low temperature based on $ZnCo_2O_4$ micro-tube sensors. *J. Hazard. Mater.* **2022**, *440*, 129753.
(40) Kim, J.; Yong, K. Mechanism Study of ZnO Nanorod-Bundle Sensors for H_2S Gas Sensing. *J. Phys. Chem. C* **2011**, *115*, 7218−7224.
(41) Hieu, N. M.; Kim, H.; Kim, C.; Hong, S.-K.; Kim, D. A Hydrogen Sulfide Gas Sensor Based on Pd-Decorated ZnO Nanorods. *J. Nanosci. Nanotechnol.* **2016**, *16*, 10351−10355.
(42) Asad, M.; Sheikhi, M. H. Highly sensitive wireless H_2S gas sensors at room temperature based on CuO-SWCNT hybrid nanomaterials. *Sens. Actuators, B* **2016**, *231*, 474−483.
(43) Wang, Y.; Wang, S.; Zhao, Y.; Zhu, B.; Kong, F.; Wang, D.; Wu, S.; Huang, W.; Zhang, S. H_2S sensing characteristics of Pt-doped α-Fe_2O_3 thick film sensors. *Sens. Actuators, B* **2007**, *125*, 79−84.
(44) Khorami, H. A.; Keyanpour-Rad, M.; Vaezi, M. R. Synthesis of SnO_2/ZnO composite nanofibers by electrospinning method and study of its ethanol sensing properties. *Appl. Surf. Sci.* **2011**, *257*, 7988−7992.
(45) Wang, Q.; Bai, J.; Huang, B.; Hu, Q.; Cheng, X.; Li, J.; Xie, E.; Wang, Y.; Pan, X. Design of $NiCo_2O_4$@SnO_2 hetero structure nanofiffiber and their low temperature ethanol sensing properties. *J. Alloys Compd.* **2019**, *791*, 1025−1032.

https://doi.org/10.1021/acsomega.3c06876
ACS Omega 2023, 8, 47023−47033